AGU PUBLICATIONS

Geophysical Research Letters

RESEARCH LETTER
10.1002/2017GL074610

Key Points:
- Polarimetric radar can detect regions of high electric fields in middle to upper levels of thunderstorms
- Lightning flash leaders follow the contours of the radar-indicated high electric field regions
- The main positive (negative) charge regions within thunderstorms lay just above (below) the radar-indicated region of high electric fields

Supporting Information:
- Supporting Information S1
- Figure S1
- Figure S2

Correspondence to:
M. I. Biggerstaff,
drdoppler@ou.edu

Citation:
Biggerstaff, M. I., Z. Zounes, A. Addison Alford, G. D. Carrie, J. T. Pilkey, M. A. Uman, and D. M. Jordan (2017), Flash propagation and inferred charge structure relative to radar-observed ice alignment signatures in a small Florida mesoscale convective system, *Geophys. Res. Lett.*, *44*, 8027–8036, doi:10.1002/2017GL074610.

Received 15 JUN 2017
Accepted 20 JUL 2017
Accepted article online 31 JUL 2017
Published online 12 AUG 2017

Flash propagation and inferred charge structure relative to radar-observed ice alignment signatures in a small Florida mesoscale convective system

Michael I. Biggerstaff[1,2,3], Zackery Zounes[1], A. Addison Alford[1], Gordon D. Carrie[1], John T. Pilkey[4], Martin A. Uman[4], and Douglas M. Jordan[4]

[1]School of Meteorology, University of Oklahoma, Norman, Oklahoma, USA, [2]Cooperative Institute for Mesoscale Meteorological Studies, University of Oklahoma, Norman, Oklahoma, USA, [3]Advanced Radar Research Center, University of Oklahoma, Norman, Oklahoma, USA, [4]Department of Electrical and Computer Engineering, University of Florida, Gainesville, Florida, USA

Abstract A series of vertical cross sections taken through a small mesoscale convective system observed over Florida by the dual-polarimetric SMART radar were combined with VHF radiation source locations from a lightning mapping array (LMA) to examine the lightning channel propagation paths relative to the radar-observed ice alignment signatures associated with regions of negative specific differential phase (K_{DP}). Additionally, charge layers inferred from analysis of LMA sources were related to the ice alignment signature. It was found that intracloud flashes initiated near the upper zero-K_{DP} boundary surrounding the negative K_{DP} region. The zero-K_{DP} boundary also delineated the propagation path of the lightning channel with the negative leaders following the upper boundary and positive leaders following the lower boundary. Very few LMA sources were found in the negative K_{DP} region. We conclude that rapid dual-polarimetric radar observations can diagnose strong electric fields and may help identify surrounding regions of charge.

Plain Language Summary Lightning is the second leading cause of meteorologically related deaths and results in billions of dollars in damage annually. Determining when a cloud becomes electrified may lead to improved warnings of lightning activity. In this paper, we show that polarimetric radar observations can reveal the location of strong electric fields in the middle to upper levels of thunderstorms. Moreover, we show that the leaders associated with intracloud lightning flashes propagate around the edges of the radar-indicated regions of high electric fields. Additionally, it was found that the main charge regions within thunderstorms follow the outer contours of the area of radar-indicated high electric fields. With the development of rapid-scanning polarimetric radar, it may be possible in the future to diagnose likely propagation paths of intracloud electrical discharges within thunderstorms.

1. Introduction

The vertical tilting of ice crystals by cloud electric fields was proposed by *Vonnegut* [1965] to explain the growth and rapid decay of visual streamers in an isolated convective cloud observed by *Hale* [1950], *Ludlam* [1950], and *Lacy* [1950]. Laboratory measurements confirmed that electric fields of 10–50 kV m^{-1} are sufficient to align particles up to 40–50 μm in major dimension, while fields ~100 kV m^{-1} can tilt particles up 0.2 to 1.0 mm in major dimension, depending on the particle habit [*Weinheimer and Few*, 1987; *Saunders and Rimmer*, 1999; *Foster and Hallett*, 2008]. In situ observations in deep cloud systems often find electric fields ~10–100 kV m^{-1} [*Simpson and Scrase*, 1937; *Marshall and Lin*, 1992; *Rust and Marshall*, 1996; *Stolzenburg et al.*, 1998; *Calhoun et al.*, 2013; *MacGorman et al.*, 2015].

Polarimetric radars have been able to observe the alignment of ice crystals by electric fields within thunderstorms [*Mendez*, 1969; *Hendry and McCormick*, 1976; *Hendry and Antar*, 1982; *Metcalf*, 1995, 1997; *Krehbiel et al.*, 1996; *Caylor and Chandrasekar*, 1996; *Scott et al.*, 2001]. As the ice crystals polarize and become aligned with the electric field, a depolarization signature in the cross-polar channel of the polarimetric radar develops [*Mendez*, 1969; *Hendry and McCormick*, 1976]. Moreover, the canting of the ice crystals causes radial decreases in differential phase in areas not dominated by large, high-density hydrometeors [*Hendry and Antar*, 1982; *Krehbiel et al.*, 1996; *Carey and Rutledge*, 1996; *Caylor and Chandrasekar*, 1996; *Scott et al.*, 2001; *Ryzhkov and Zrnić*, 2007]. For centimeter-wave radar systems, the canting produces a greater signal

in differential phase than differential attenuation. This signature diminishes quickly after an electrical discharge, as the time required for ice plates and columns to align aerodynamically is on the order of 10 ms [*Cho et al*., 1981].

While previous studies [*Metcalf*, 1995, 1997; *Krehbiel et al*., 1996; *Scott et al*., 2001] have illustrated the instantaneous vertical cloud structure associated with electrically aligned ice particle signatures, the evolution of the spatial pattern of these signatures has not been well documented. More importantly, coincident measurements of the ice alignment radar signature to flash propagation and the location of the primary charge layers within the cloud have not yet been thoroughly examined.

In this study, a series of vertical cross sections taken through a small mesoscale convective system (MCS) observed over Florida by a C band dual-polarimetric radar are combined with VHF radiation source locations from a lightning mapping array (LMA) [*Rison et al*., 1999] to illustrate the lightning channel propagation paths relative to the radar-observed ice alignment signatures. Additionally, charge layer locations, inferred from analysis of the LMA sources following the method of *Thomas et al*. [2002], *Hamlin* [2004], *Marshall et al*. [2005], *Wiens et al*. [2005], and *Weiss et al*. [2008], are related to the radar observed alignment signature. The sample period of the radar cross sections (every ~20 s) is consistent with the volume sampling times of phased-array radars [*Heinselman et al*., 2008; *Isom et al*., 2013; and *French et al*., 2014]. Hence, this study also demonstrates the utility of rapid scanning radar systems for mapping the primary charge regions within convective cloud systems.

2. Data

The storm of interest was observed over north central Florida on 17 July 2012 from 1936 to 2121 UTC by the C band dual-polarimetric Shared Mobile Atmospheric Research and Teaching (SMART) radar [*Biggerstaff et al*., 2005] deployed at the Keystone Heights Airpark in support of the International Center for Lightning Research and Testing (ICLRT) triggered lightning experiments [e.g., *Hill et al*., 2013; *Pilkey et al*., 2013, 2014; *MacGorman et al*., 2015; *Hare et al*., 2016]. The radar operated in simultaneous transmit and receive (STaR) mode [*Doviak et al*., 2000; *Scott et al*., 2001], collecting a sector volume of five range-height indicator (RHI) scans (vertical cross section) spaced 1° apart in azimuth and centered over the ICLRT every 120 s. Each vertical scan took about 20 s to complete. The ICLRT was located 11.6 km at an azimuth of 10.5° from the radar. Thus, at the range of the ICLRT, the azimuthal spacing between RHIs was ~200 m. Manual editing of the data was performed to remove noisy values of K_{DP} from the edges of the precipitation echo.

The seven-station ICLRT LMA network for this event was described by *Pilkey et al*. [2014]. In this study, we used only those LMA radiation sources that had at least five-station solutions with low chi-square values ("goodness of fit") of 1.0 or less.

The WSR-88D radar is located at the Jacksonville, FL, International Airport on the northern edge of the city at a range of 68 km to the north-northeast of the ICLRT. Only the base reflectivity scans are used here.

3. Results

3.1. Storm Overview

Base reflectivity from the WSR-88D radar (Figure 1) showed that the 17 July 2012 storm was a small leading-line trailing-stratiform squall line system similar to that studied by *Biggerstaff and Houze* [1991a, 1991b, 1993], *Sun et al*. [1993], and *Lund et al*. [2009]. At 2053 UTC, the main convective region had just moved past the ICLRT (Figure 1a). The gust front, associated with the fine line of radar reflectivity to the north of the convective band, surged northward, reducing the depth of the low-level convergence and leading to a weakening of the convective cells within the main body of the system. By 2140 UTC the convection around ICLRT was in the dissipating stages (Figure 1d) although the gust front was able to generate additional, relatively isolated, convection about 30–40 km to the northwest and northeast.

The precipitation trailing the main convective band consisted initially of older, dissipating convective cells but was later augmented by storm-relative front-to-rear flow to produce a more horizontally uniform reflectivity structure.

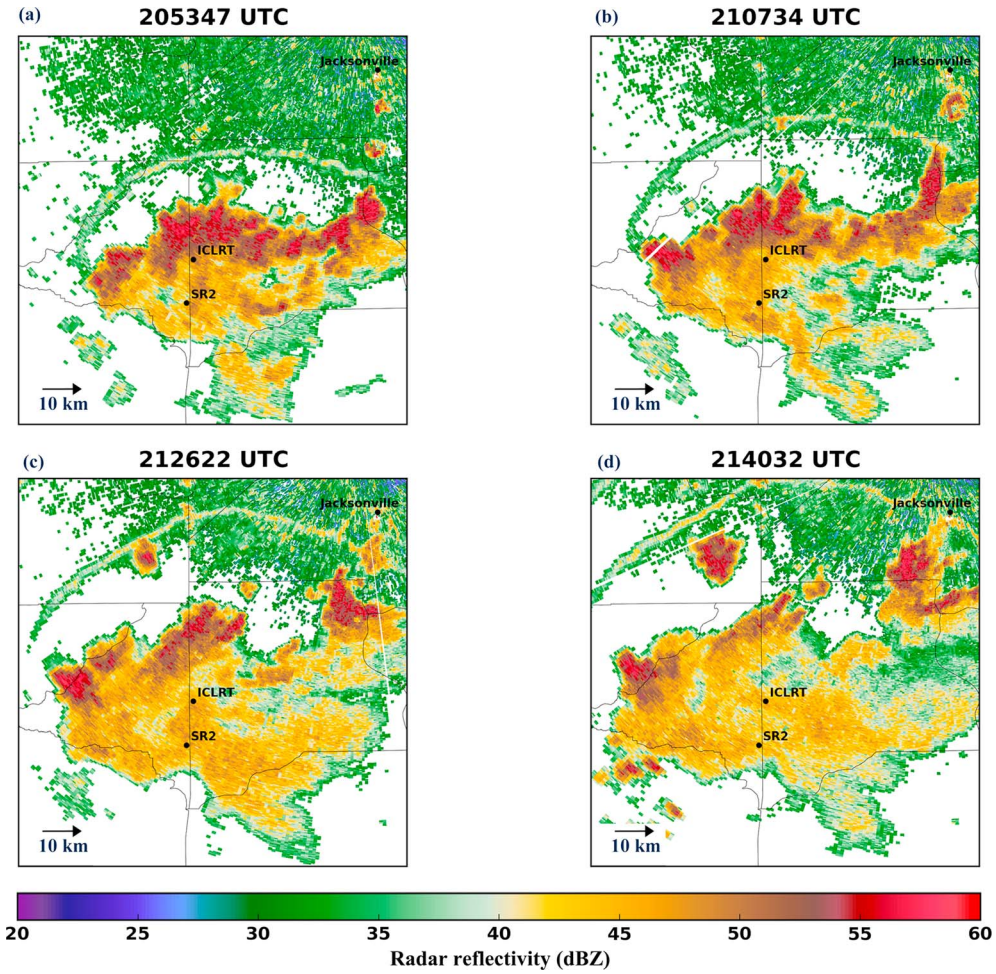

Figure 1. Base (0.5° elevation) PPI scans of radar reflectivity (in dBZ, according to the color scale) from the Jacksonville, FL, WSR-88D radar at (a) 2053:47 UTC, (b) 2107:34 UTC, (c) 2126:22 UTC, and (d) 2140:32 UTC on 17 July 2012. The position of the SR2 SMART radar, the ICLRT, and the city center of Jacksonville are provided for reference.

3.2. Individual Flash Propagation Relative to Storm Structure

The flash rate of the storm system, ~10 min^{-1} within 30 km of ICLRT [*Pilkey et al.*, 2014], was faster than the individual RHI scanning rate of the radar system. Ice alignment signatures diminish rapidly in response to an electrical discharge but can rebuild in the same general area over a period of several seconds [*Hendry and Antar*, 1982]. Additionally, many of the flashes observed here had some component of propagation perpendicular to the radar cross sections. To reduce short time and spatial scale fluctuations and to better represent the ice alignment signature relative to individual flashes, a five-RHI mean cross section was constructed centered on the RHI closest in time to but prior to an electrical discharge. Only those flashes that are within 5 km, horizontally, of the mean RHI, with most of the sources lying quasi-parallel to the RHI orientation, were examined.

The results of the analysis can be represented by two examples. The first was taken at a mean time of 1953:01 UTC during the early stage of the MCS (Figures 2a–2c), when the convective system had little trailing precipitation and the convective cells were most vigorous in terms of echo tops, which approached 12 km, close to the maximum 13 km observed at 2000 UTC (Figure 2a). Two main regions associated with the vertical tilting of ice crystals by the cloud's electric fields are evident in the specific differential phase (Figure 2b). When ice crystals are oriented aerodynamically, there is weakly positive (green color in Figures 2 and 3) differential phase shift. Where the crystals are canted vertically (e.g., due to alignment with the vertical component of the electric field), the differential phase decreases (cf. Figures S1 and S2 in the supporting information) [see also *Krehbiel et al.*, 2005], creating a region of negative K_{DP} (yellow color in Figures 2 and 3). The

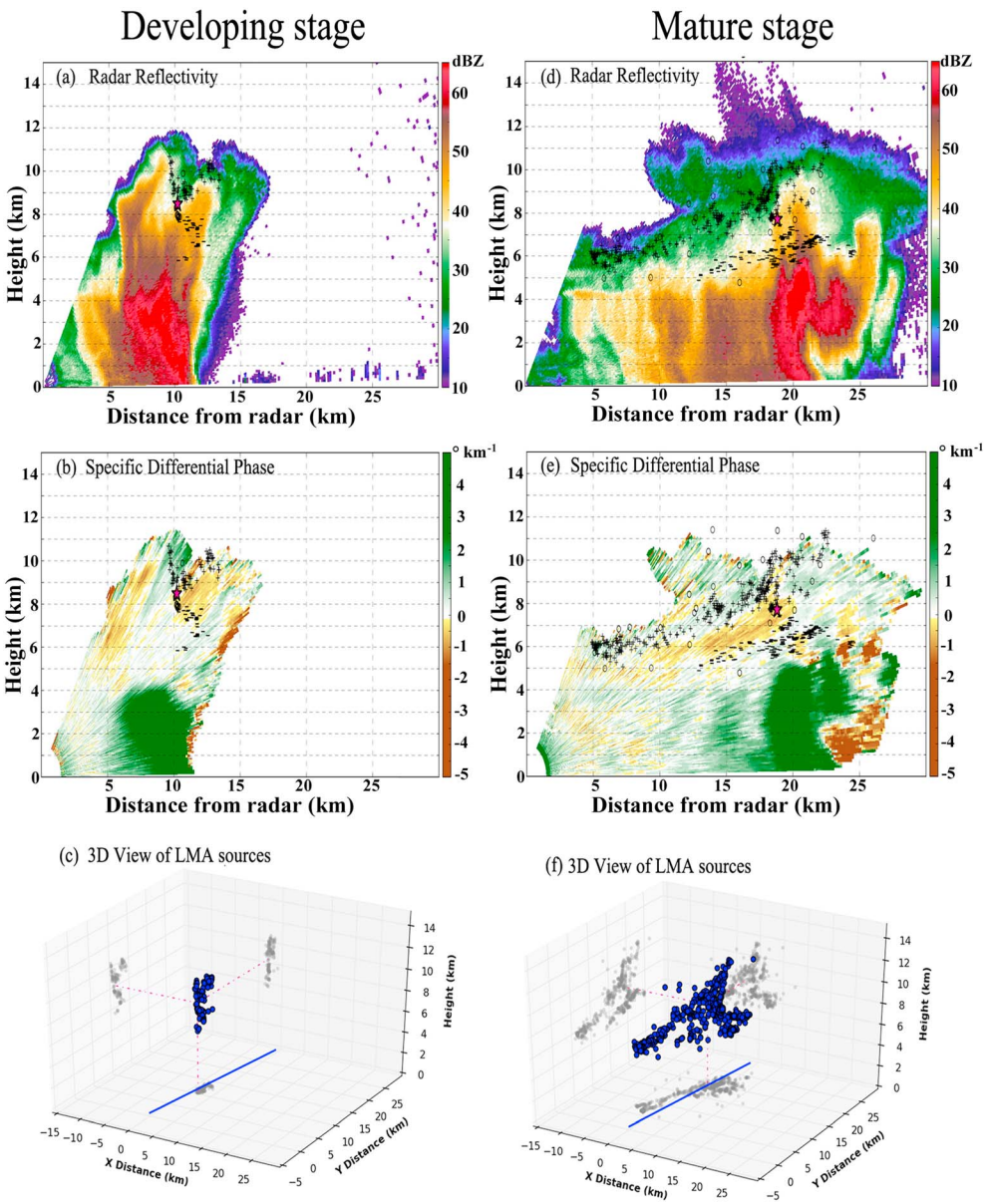

Figure 2. On the left side, developing-stage volume mean (a) radar reflectivity (in dBZ, according to the color scale) and (b) specific differential phase (in ° km^{-1}, according to the color scale) for the volume with a mean time of 1953:01 UTC. The projection of LMA sources for an intracloud flash that occurred 25 s after the radar volume mean time is overlaid on the center plane of the radar scan (10.5° azimuth). (c) The 3-D structure of the flash. On the right side, mature-stage volume mean (d) radar reflectivity and (e) specific differential phase for the volume with a mean time of 2039:25 UTC. The projection of LMA sources for an intracloud flash that occurred 18 s after the radar volume mean time is overlaid. (f) The 3-D structure of the flash. In Figures 2a, 2b, 2d, and 2e, the red star indicates the flash initiation point, radiation sources that are within inferred negative (positive) charge regions are plotted with dash (cross) symbols, while open circles represent sources moving through undetermined charge. The blue line Figures 2c and 2f represents the mean azimuth angle of the volume and is along the line between the SMART radar and the ICLRT.

negative K_{DP} regions are the ice alignment radar signatures. Hence, the two broad regions of negative K_{DP}, one elongated and centered near (x, z) of (6, 7) km and the other circular and centered near (11, 8) km, indicate regions in which the vertical component of the electric field is particularly strong.

It is important to consider that the negative K_{DP} areas in Figure 2 could be caused by backscatter from conical graupel, as the region had relatively high radar reflectivity (>35 dBZ). Conical graupel can produce negative

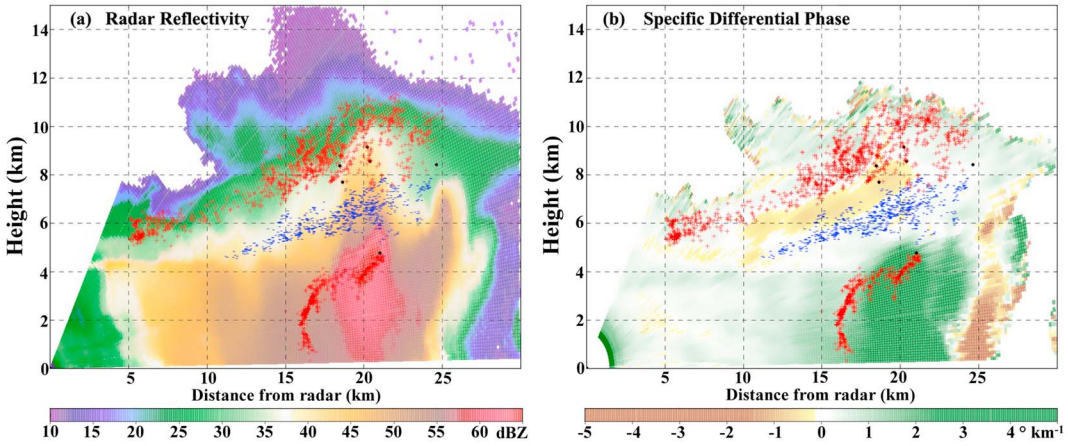

Figure 3. Time-averaged mean (a) radar reflectivity, in dBZ according to the color scale, and (b) specific differential phase, in degrees per kilometer according to the color scale, for the time period of 2034:14 through 2042:25 UTC. LMA sources for the six analyzed flashes observed during this period are overlaid. The red crosses (blue dashes) indicated regions of inferred positive (negative) charge.

K_{DP}, since it falls with a preferred vertical orientation [*Zikmunda and Vali*, 1972]; however, the differential radar reflectivity (Z_{DR}) is typically negative for conical graupel [*Oue et al*., 2015; *Bringi et al*., 2017] and only near zero to weakly positive Z_{DR} was observed here (not shown). Hence, we believe this radar ice alignment signature is denoting a region of particularly strong (~100 kV m^{-1}) electric field aloft since it is able to produce an ice alignment signature in what must be a combination of graupel, aggregates, and smaller crystals.

Negative K_{DP} regions may also be associated with rainfall-to-clear air gradients along the far edges of precipitation regions. To mitigate amplification of the inherent noise in the measured differential phase, K_{DP} is determined from the slope of a local, centered, least squares linear fit of differential phase [cf., *Wang and Chandrasekar*, 2009]. At the far edges of a precipitation core, the least squares window includes large values of differential phase, which may be augmented by resonance effects [*Hubbert et al*., 1993], associated with the nearby rain followed by random values of differential phase associated with noise in the nonprecipitation region. Since differential phase accumulates with range, the distribution of random noise would be biased low relative to the last rainy values of differential phase. Hence, even neglecting resonance effects, the slope of the least squares fit will be negative, resulting in negative K_{DP} on the far edges of precipitation regions and between cores of thunderstorm cells when there is a lack of precipitation between the cells. Both mean cross sections of K_{DP} (Figures 2b and 2e) exhibit these rainfall gradient artifacts along the far edges of the storm.

Using a one-dimensional approximation to Gauss's law [e. g., *Marshall and Rust*, 1991], the charge density is given by the product of the air permittivity and the height gradient of the vertical component of the electric field. Consequently, assuming a normal-polarity tripole charge distribution [*Simpson and Robinson*, 1941] with the main positive charge layer just above the primary negative charge layer and a weaker positive charge layer farther below, the strongest electric field (and region of negative K_{DP}) would reside between the primary negative and upper positive charge layers, similar to the profile of electric field shown in *Lund et al*. [2009]. The electric field would weaken toward the middle of the charge layers. Hence, positive K_{DP} areas surrounding the negative K_{DP} region would indicate that part of the charge layer where the electric fields are too small to tilt ice crystals. If the negative K_{DP} regions delineate local extrema in electric fields, then those areas also delineate regions with zero or weak magnitudes of charge density. Since the magnitude of vertical gradient of the electric field increases between the negative and surrounding positive K_{DP} regions, then the area between the positive and negative K_{DP} regions would have higher charge density than the negative K_{DP} region itself. Exactly where the *maximum* in charge density resides is not clear. It may lie farther within the positive K_{DP} regions that surround the negative K_{DP} area. Hence, the lightning channel can continue to propagate into possibly greater charge density in the positive K_{DP} regions surrounding the negative K_{DP} area.

The LMA radiation sources from an intracloud lightning flash that occurred 25 s after the mean volume time and close to the mean RHI orientation (Figure 2c) is overlaid on the K_{DP} field in Figure 2b. Following *Maggio et al*. [2005], the initial LMA source with low chi-square (good location fit) is used to determine the flash initiation location. The flash appeared to initiate at 8.5 km altitude near the edge of the upper boundary around the circular negative K_{DP} region. Most of the flashes analyzed for this case exhibited similar initiation locations —near the upper boundary but slightly within the negative K_{DP} region. The remaining flashes were closer to the zero K_{DP} contour adjacent to the region of negative K_{DP} or slightly within the surrounding positive region. Regardless, it is clear that the apparent initiation location is near the radar-indicated region with strong electric fields, in agreement with the view that flashes initiate near the maximum electric field as described by *Kasemir* [1960] and *Mazur and Ruhnke* [1993, 1998].

Two other aspects of the lightning propagation are evident. First, the inferred positive leaders moving through negative charge generally follow the near-zero K_{DP} boundary along the lower edge of the ice alignment signature. This structure was prominent in almost all of the intracloud flashes analyzed here. Given that a flash acts to increase the complexity of the local electric field [*Coleman et al*., 2003] and the radar sample time is slow compared to the flash rate, exceptions to this structure may be due to poorly synced observations. The near zero or weakly positive K_{DP} boundary surrounding an ice alignment signature may mark an area with high charge density. Thus, it appears that the positive breakdown path follows a region of strong charge, in agreement with *Shao and Krehbiel* [1996], *Marshall and Stolzenburg* [2002], *Coleman et al*. [2003] and *Riousset et al*. [2007]. Indeed, as found by *Coleman et al*. [2003], the path appears to be on the near side of an extremum in charge (the side closest to the other half of the flash) since most of the radiation sources are located in the near-zero K_{DP} boundary which would imply some degree of ice particle canting. Second, the path of the inferred negative leaders moving through positive charge generally travels around the upper K_{DP} boundary surrounding the ice alignment signature and onward through regions of positive K_{DP}, which is the aerodynamically preferred value that would be associated with noncanted ice particles in areas with weak electric fields. Most of the intracloud flashes analyzed here had at least one negative leader branch that terminated along the edges of the precipitation field.

The second example that typifies our analysis was taken at a center time of 2039:25 UTC, during the mature stage of the MCS (Figures 2d–2f). The sloped nature of radar reflectivity values behind the main convective cells, which were located near 20 km range from the radar (Figure 2d), reveals that the trailing precipitation region was mainly comprised of dissipating convective cells. A radar bright band, indicative of melting, was starting to form in the more horizontally stratified echo within 7 km range from the radar. The K_{DP} field reveals a broad region associated with ice alignment that was centered at (17, 7) km (Figure 2e) with smaller pockets of negative K_{DP} to the rear and beneath the main region of strong electric field. Due to the increasingly dissipative stages of the old convective cells, the negative K_{DP} region exhibits a downward slope toward the back of the squall line. *Pilkey et al*. [2014] observed a similar downward slope in the inferred charge regions of this and others cases and related this structure to charge advection and sedimentation [*Stolzenburg et al*., 1998].

Similar to the previous example, the flash initiated within the radar-inferred region of strong electric field (negative K_{DP} area) between the inferred upper positive and lower negative charge regions (Figure 2e). This intracloud flash, which occurred 18 s after the center five RHI time, was more horizontally extensive than the earlier intracloud flash and existed over a greater depth of the cloud (from 4.3 to 11.5 km altitude; compare Figures 2c and 2f). The inferred negative leader traversed a positive charge layer that apparently lay above the upper boundary of and followed the downward slope of the negative K_{DP} region toward the rear of the storm system. The negative leader radiation sources also followed the contours of radar reflectivity that separated reflectivity greater than 35 dBZ from lower values aloft. It is likely that the backscatter in the higher reflectivity below was dominated by high-density rimed ice particles, such as graupel, while the weaker reflectivity aloft, in which the positive charge was found, was dominated by low-density ice aggregates.

As before, the radiation sources associated with the positive leader portion of the flash followed the lower boundary of the negative K_{DP} ice alignment signature. In this example, some of the radiation sources traveled through an area of weakly positive K_{DP} before following the boundary of another, smaller negative K_{DP} region found at (20.5, 6) km (Figure 2e). The tendency for part of the flash to follow the boundary of

smaller K_{DP} ice alignment signatures suggests that the radar may be able to detect small pockets of strong fields (and associated inferred neighboring charge areas) in addition to the larger, more horizontally extensive electric fields.

3.3. Inferred Charge Layers in Relation to Time-Averaged Ice Alignment Signature

To further elucidate the correspondence between radar-inferred regions of strong electric fields associated with negative K_{DP} ice alignment signatures and LMA-inferred charge layers within the storm system, sets of six flashes were analyzed and overlaid on the mean storm structure for the time period associated with the six flashes. For a flash to be considered, the majority of LMA sources had to be within 5 km of the mean RHI orientation, the flash had to have enough sources to be easily analyzed (>80 sources), and the orientation of the flash had to be quasi-parallel to the mean RHI orientation.

The mean storm structure and analyzed charge regions for an ~8 min period during the mature stage of the MCS is shown in Figure 3. Immediately striking is the near dearth of LMA radiation sources in the region of high electric field as indicated by the sloping negative K_{DP} ice alignment signature that extended from the mature cells in the convective region rearward to the back of the storm toward the radar (Figure 3b). The vast majority of the sources in the negative charged layer (blue dashes in Figure 3) were found along the bottom boundary of the ice alignment signature, near zero to weakly positive K_{DP} values. The layer of inferred negative charge follows the contours of the ice alignment signature, sloping downward from a center at 7 km in altitude in the convection to just above the melting level (4.5 km) in the developing stratiform region at the rear of the cross section.

The LMA-inferred layer of upper positive charge (red crosses in Figure 3) also slopes downward in conjunction with the negative K_{DP} region. The upper positive charge layer is centered near 10 km altitude in the convective region and about 6 km altitude in the developing stratiform region.

Both of the charge layers seem to exist within preferred reflectivity bands (Figure 3a). In the dissipating convective cells and the transition zone [*Biggerstaff and Houze*, 1993] (i.e., for precipitation within 17 km range of the radar), the negative charge layer lays mainly within a band of 40 ± 3 dBZ, likely associated with moderately sized graupel that is not wet enough to produce higher reflectivity. The upper positive charge layer follows the slope of the 30–35 dBZ reflectivity band, which is consistent with large aggregates of crystals. The upper reflectivity band may also be fortuitous as there was a sharp gradient in reflectivity denoting the upper boundary of the precipitation region. A deeper stratiform layer would be needed to determine if the upper positive charge layer reflectivity values are meaningful.

A negative cloud-to-ground flash was included in the set of six flashes shown in Figure 3. Analysis of the flash indicated that these radiation sources were associated with a negative leader and passed through a lower positive charge layer that is consistent with the commonly observed tripole charge structure [*Simpson and Robinson*, 1941; *Williams*, 1989; *Bruning et al*., 2010]. The bottom boundary of the lower positive charge region was undeterminable; therefore, all the flash sources are marked as positive charge to denote that the leader was negative. Regardless, given that the lower charge region laid within an area of high reflectivity associated with large wet, melting, ice particles or rain drops, all of which would produce relatively large positive K_{DP} values, no ice alignment signature would be expected to be found. Indeed, the radar-inferred electrical structure appears to be best suited for analyzing electric fields that would be involved with intracloud rather than cloud-to-ground flashes.

4. Conclusions

Dual-polarimetric SMART radar data were combined with LMA VHF radiation sources to relate the lightning propagation paths and inferred charge structure to the negative specific differential phase (K_{DP}) radar signature of ice alignment by strong electric fields. We found that initiation of intracloud flashes occurred in close proximity to the upper zero-K_{DP} boundary surrounding the negative K_{DP} region. The positive leaders moving through negative charge followed the bottom of the negative K_{DP} region. Similarly, the negative leaders moving through positive charge followed the upper boundary of the negative K_{DP} region and onward into weakly positive K_{DP} that would be associated with weak electric fields but presumably areas of higher charge density. This structure was evident for individual flashes as well as composites of flashes when compared to ~100 s and ~8 min time-averaged storm structure.

For the intracloud flashes analyzed here, at least one branch of the negative leader terminated at an upper level precipitation boundary of the storm. The positive leader appeared to terminate within the precipitation. Since both leaders followed the orientation of the zero-K_{DP} boundary, it appears that the flash propagates into high charge density on the near side of a potential well, as described by *Coleman et al.* [2003]. Indeed, there were very few LMA sources within the negative K_{DP} region that marked areas of strong electric fields and weak charge density.

During the mature stage of the MCS, the inferred charge layers followed the slope of the negative K_{DP} region from the back of the convective region to the observed rear of the precipitation system. Additionally, the charge layers appeared to lie within preferred reflectivity ranges that separated backscatter dominated by low-density aggregates from that dominated by higher-density graupel.

The rapid sampling of high vertical resolution data from polarimetric radar was able to delineate regions of strong electric fields and help identify likely areas of high charge density surrounding those fields in the middle to upper levels of the clouds where ice crystals and small aggregates exist that can be tilted by the electrostatic fields. It is important to note that the negative K_{DP} radar signature appears in regions where there is a combination of appropriate hydrometeors (ice particles) and the necessary magnitude of the electric field needed to align them. In the future, as polarimetric phased array radars become commonplace, it may be possible to apply the relationships elucidated here to identify probable propagation paths of intracloud flashes.

Acknowledgments
This work was supported by the National Science Foundation under grant AGS-1063537 and the DARPA Nimbus project. Data used here are available at doi:10.5281/zenodo.809446.

References

Biggerstaff, M. I., and R. A. Houze Jr. (1991a), Kinematic and precipitation structure of the 10–11 June 1985 squall line, *Mon. Wea. Rev.*, *119*, 3034–3065, doi:10.1175/1520-0493(1991)119<3034:KAPSOT>2.0.CO;2.

Biggerstaff, M. I., and R. A. Houze Jr. (1991b), Midlevel vorticity structure of the 10–11 June 1985 squall line, *Mon. Wea. Rev.*, *119*, 3066–3079, doi:10.1175/1520-0493(1991)119<3066:MVSOTJ>2.0.CO;2.

Biggerstaff, M. I., and R. A. Houze Jr. (1993), Kinematics and microphysics of the transition zone of the 10–11 June, 1985 squall-line system, *J. Atmos. Sci.*, *50*, 3091–3110, doi:10.1175/1520–0469(1993)050<3091:KAMOTT>2.0.CO;2.

Biggerstaff, M. I., L. J. Wicker, J. Guynes, C. Ziegler, J. M. Straka, E. N. Rasmussen, A. Dogget IV, L. D. Carey, J. L. Schroeder, and C. Weiss (2005), The Shared Mobile Atmospheric Research and Teaching (SMART) radar: A collaboration to enhance research and teaching, *Bull. Amer. Meteor. Soc.*, *86*, 1263–1274, doi:10.1175/BAMS-86-9-1263.

Bringi, V. N., P. C. Kennedy, G.-J. Huang, C. Kleinkort, M. Thurai, and B. M. Notaros (2017), Dual-polarized radar and surface observations of a winter graupel shower with negative Z_{dr} column, *J. Appl. Meteor. Climate*, doi:10.1175/JAMC-D-16-0197.1.

Bruning, E. C., W. D. Rust, D. R. MacGorman, M. I. Biggerstaff, and T. Schuur (2010), Formation of charge structures in a supercell, *Mon. Weather Rev.*, *138*, 3740–3761, doi:10.1175/2010MWR3160.1.

Calhoun, K. M., D. R. MacGorman, C. L. Ziegler, and M. I. Biggerstaff (2013), Evolution of lightning activity and storm charge relative to dual-Doppler analysis of a high precipitation supercell storm, *Mon. Weather Rev.*, *141*, 2199–2223, doi:10.1175/MWR-D-12-00258.1.

Carey, L. D., and S. A. Rutledge (1996), A multiparameter radar case study of the microphysical and kinematic evolution of a lightning producing storm, *Meteorl. Atmos. Phys.*, *59*, 33–64, doi:10.1007/BF01032000.

Caylor, I. J., and V. Chandrasekar (1996), Time-varying ice crystal orientation in thunderstorms observed with multiparameter radar, *IEEE Trans, Geosci. Rem. Sens.*, *34*, 847–858, doi:10.1109/36.508402.

Cho, H-R., J. V. Iribarne, and W. G. Richards (1981), On the orientation of ice crystals in a cumulonimbus cloud, *J. Atmos. Sci.*, *38*, 1111–114, doi:10.1175/1520-0469(1981)038<1111:OTOOIC>2.0.CO;2.

Coleman, L. M., T. C. Marshall, M. Stolzenburg, T. Hamlin, P. R. Krehbiel, W. Rison, and R. J. Thomas (2003), Effects of charge and electrostatic potential on lightning propagation. *J. Geophys. Res.*, *108*(D9), 4298, doi:10.1029/2002JD002718.

Doviak, R. J., V. N. Bringi, A. Ryzhkov, A. Zahrai, and D. S. Zrnic (2000), Considerations for polarimetric upgrades to operational WSR-88D radars, *J. Atmos. Oceanic Technol.*, *17*, 257–278, doi:10.1175/1520-0426(2000)017<0257:CFPUTO>2.0.CO;2.

Foster, T. C., and J. Hallett (2008), Enhanced alignment of plate ice crystals in a non-uniform electric field, *Atmos. Res.*, *90*, 41–53.

French, M. M., H. B. Bluestein, I. PopStefanija, C. A. Baldi, and R. T. Bluth (2014), Mobile, phased-array, Doppler radar observations of tornadoes at X band, *Mon. Weather Rev.*, *142*, 1010–1036, doi:10.1175/MWR-D-13-00101.1.

Hale, R. B. (1950), Unusual lightning, *Weather*, *4*, 394.

Hamlin, T. (2004), The New Mexico Tech lightning mapping array, PhD Dissert., New Mexico Inst. Mining and Technol., 183.

Hare, B. M., et al. (2016), Ground-level observation of a terrestrial gamma ray flash initiated by a triggered lightning, *J. Geophys. Res. Atmos.*, *121*, 6511–6533, doi:10.1002/2015JD024426.

Heinselman, P. L., D. L. Priegnitz, K. L. Manross, T. M. Smith, and R. W. Adams (2008), Rapid sampling of severe storms by the National Weather Radar Testbed Phased Array Radar, *Weather Forecasting*, *23*, 808–824, doi:10.1175/2008WAF2007071.1.

Hendry, A., and G. C. McCormick (1976), Radar observations of the alignment of precipitation particles by electrostatic fields in thunderstorms, *J. Geophys. Res.*, *81*, 5353–5357, doi:10.1029/JC081i030p05353.

Hendry, A., and Y. M. M. Antar (1982), Radar observations of polarization characteristics and lightning-induced realignment of atmospheric ice crystals, *Radio Sci.*, *17*, 1243–1250, doi:10.1029/RS017i005p01243.

Hill, J. D., J. Pilkey, M. A. Uman, D. M. Jordan, W. Rison, P. R. Krehbiel, M. I. Biggerstaff, P. Hyland, and R. Blakeslee (2013), Correlated lightning mapping array and radar observations of the initial stages of three sequentially triggered Florida lightning discharges, *J. Geophys. Res. Atmos.*, *118*, 8460–8481, doi:10.1002/jgrd.50660.

Hubbert, J., V. Chandrasekar, V. N. Bringi, and P. Meischner (1993), Processing and interpretation of coherent dual-polarized radar measurements, *J. Atmos. Oceanic Technol.*, *10*, 155–164, doi:10.1175/1520-0426(1993)010<0155:PAIOCD>2.0.CO;2.

Isom, B., R. Palmer, R. Kelley, J. Meier, D. Bodine, M. Yeary, B.-L. Cheong, Y. Zhang, T. Y. Yu, and M. I. Biggerstaff (2013), The atmospheric imaging radar: Simultaneous volumetric observations using a phased array weather radar, *J. Atmos. Oceanic Technol.*, *30*, 655–675, doi:10.1175/JTECH-D-12-00063.1.

Kasemir, H. W. (1960), A contribution to the electrostatic theory of a lightning discharge, *J. Geophys. Res.*, *65*, 1873–1878, doi:10.1029/JZ065i007p01873.

Krehbiel, P., T. Chen, S. McCrary, W. Rison, G. Gray, and M. Brook (1996), The use of dual channel circular-polarization radar observations for remotely sensing storm electrification, *Meteorl. Atmos. Phys.*, *59*, 65–82, doi:10.1007/BF01032001.

Krehbiel, P., W. Rison, R. J. Thomas, C. Maggio, T. Marshall, M. Stolzenberg, T. Hamlin, and K. Wiens (2005), Lightning and dual-polarization radar structure of small convective storms. Proc., 32nd Conf. Radar Meteor., Amer. Meteor. Soc., Albuquerque, NM, USA, 15R.2.

Lacy, R. E. (1950), Unusual lightning, *Weather*, *4*, 395.

Ludlam, F. H. (1950), Unusual lightning, *Weather*, *4*, 494.

Lund, N. R., D. R. MacGorman, T. J. Schuur, M. I. Biggerstaff, and W. D. Rust (2009), Relationships between lightning location and polarimetric radar signatures in a small mesoscale convective system, *Mon. Wea. Rev.*, *137*, 4151–4170, doi:10.1175/2009MWR2860.1.

MacGorman, D. R., M. I. Biggerstaff, S. Waugh, J. T. Pilkey, M. A. Uman, D. M. Jordan, T. Ngin, W. R. Gamerota, G. Carrie, and P. Hyland (2015), Coordinated lightning, balloon-borne electric field and radar observations of triggered lightning flashes in north Florida, *Geophsy. Res. Lett.*, *42*, 5635–5643, doi:10.1002/2015GL064203.

Maggio, C., L. Coleman, T. Marshall, M. Stolzenburg, M. Stanley, T. Hamlin, P. Krehbiel, W. Rison, and R. Thomas (2005), Lightning-initiation locations as a remote sensing tool of large thunderstorm electric field vectors, *J. Atmos. Ocean. Technol.*, *22*, 1059–1068, doi:10.1175/JTECH1750.1.

Marshall, T. C., and B. Lin (1992), Electricity in dying thunderstorms, *J. Geophys. Res.*, *97*, 9913–9918, doi:10.1029/92JD00463.

Marshall, T. C., and W. D. Rust (1991), Electric field soundings through thunderstorms, *J. Geophys. Res.*, *96*, 22,297–22,306, doi:10.1029/91JD02486.

Marshall, T. C., and M. Stolzenburg (2002), Electrical energy constraints on lightning. *J. Geophys. Res.*, *107*(D7), 4052, doi:10.1029/2000JD000024.

Marshall, T. C., M. Stolzenburg, C. R. Maggio, L. M. Coleman, P. R. Krehbiel, T. Hamlin, R. J. Thomas, and W. Rison (2005), Observed electric fields associated with lightning initiation, *Geophys. Res. Lettrs.*, *32*, L03813, doi:10.1029/2004GL021802.

Mazur, V., and L. H. Ruhnke (1993), Common physical processes in natural and artificially triggered lightning, *J. Geophys. Res.*, *98*, 12,913–12,930, doi:10.1029/93JD00626.

Mazur, V., and L. H. Ruhnke (1998), Model of electric charges in thunderstorms and associated lightning, *J. Geophys. Res.*, *103*, 23,299–23,308, doi:10.1029/98JD02120.

Mendez, D. J. (1969), Optical polarization induced by electric fields of thunderstorms, *J. Geophys. Res.*, *74*, 7032–7037, doi:10.1007/BF01249599.

Metcalf, J. I. (1995), Radar observations of changing orientations of hydrometeors in thunderstorms, *J. Appl. Meteor.*, *34*, 757–772, doi:10.1175/1520-0450(1995)034<0757:ROOCOO>2.0.CO;2.

Metcalf, J. I. (1997), Temporal and spatial variations of hydrometeor orientations in thunderstorms, *J. Appl. Meteorol.*, *36*, 315–321, doi:10.1175/1520-0450(1997)036<0315:TASVOH>2.0.CO;2.

Oue, M., M. R. Kumjian, Y. Lu, Z. Jiang, E. Clothiaux, J. Verlinde, and K. Aydin (2015), X-band polarimetric and Ka-band observations of graupel-producing Artic mixed-phase cloud, *J. Appl. Meteor. Climo.*, *54*, 1335–1351, doi:10.1175/JAMC-D-14-0315.1.

Pilkey, J., et al. (2013), Rocket-and-wire triggered lightning in 2012 tropical storm Debby in the absence of natural lightning, *J. Geophys. Res. Atmos.*, *118*, 13,158–13,174, doi:10.1002/2013JD020501.

Pilkey, J. T., M. A. Uman, J. D. Hill, T. Ngin, W. R. Gamerota, D. M. Jordan, J. Caicedo, and B. Hare (2014), Rocket-triggered lightning paths relative to preceding natural lightning activity and inferred cloud charge, *J. Geophys. Res. Atmos.*, *119*, 13,427–13,446, doi:10.1002/2014JD022139.

Riousset, J. A., V. P. Pasko, P. R. Krehbiel, R. J. Thomas, and W. Rison (2007), Three-dimensional fractal modeling of intracloud lightning discharge in a New Mexico thunderstorm and comparison with lightning mapping observations, *J. Geophys. Res.*, *112*, D15203, doi:10.1029/2006JD007621.

Rison, W., P. R. Krehbiel, T. Hamlin, and J. Harlin (1999), A GPS-based three-dimensional lightning mapping system: Initial observations in central New Mexico, *Geophys. Res. Lettrs.*, *26*, 3573–3576, doi:10.1029/1999GL010856.

Rust, W. D., and T. C. Marshall (1996), On abandoning the thunderstorm tripole-charge paradigm, *J. Geophys. Res.*, *101*, 23,499–23,504, doi:10.1029/96JD01802.

Ryzhkov, A. V., and D. S. Zrnić (2007), Depolarization in ice crystals and its effect on radar polarimetric measurements, *J. Atmos. Ocean. Technol.*, *24*, 1256–1267, doi:10.1175/JTECH2034.1.

Saunders, C. P. R., and J. S. Rimmer (1999), The electric field alignment of ice crystals in thunderstorms, *Atmos. Research*, *51*, 337–343, doi:10.1016/S0169-8095(99)00018-6.

Scott, R. D., P. R. Krehbiel, and W. Rison (2001), The use of simultaneous horizontal and vertical transmissions for dual-polarization radar meteorological observations, *J. Atmos. Ocean. Technol.*, *18*, 629–648, doi:10.1175/1520-0426(2001)018<0629:TUOSHA>2.0.CO;2.

Shao, X. M., and P. R. Krehbiel (1996), The spatial and temporal development of intracloud lightning, *J. Geophys. Res.*, *101*, 26,641–26,668, doi:10.1029/96JD01803.

Simpson, G., and F. J. Scrase (1937), The distribution of electricity in thunderclouds, *Proc. R. Soc. London*, 309–352, doi:10.1098/rspa.1937.0148.

Simpson, G., and G. D. Robinson (1941), The distribution of electricity in thunderclouds, II, *Proc. Royal Soc. A.*, *177*, 281–329.

Stolzenburg, M., W. D. Rust, and T. C. Marshall (1998), Electrical structure in thunderstorm convective regions: 1. Mesoscale convective systems, *J. Geophys. Res.*, *103*, 14,059–14,079, doi:10.1029/97JD03547.

Sun, J., S. Braun, R. G. Fovell, M. I. Biggerstaff, and R. A. Houze Jr. (1993), Warm upper-level downdrafts associated with a squall line, *Mon. Wea. Rev.*, *121*, 2919–2927, doi:10.1175/1520-0493(1993)121<2919:WULDAW>2.0.CO;2.

Thomas, R. J., S. Behnke, T. Hamlin, J. Harlin, P. Krehbiel, W. Rison (2002), New Mexico thunderstorms observed by the lightning mapping array: An overview of one season, *Eos Trans. AGU*, *83*(47), Fall Meet. Suppl., Abstract A71B-0097.

Vonnegut, B. (1965), Orientation of ice crystals in the electric field of a thunderstorm, *Weather*, *20*, 310–312, doi:10.1002/j.1477-8696.1965.tb02740.x.

Wang, Y., and V. Chandrasekar (2009), Algorithm for estimation of specific differential phase, *J. Atmos. Oceanic Technol.*, *26*, 2565–2578, doi:10.1175/2009JTECHA1358.1.

Weinheimer, A. J., and A. A. Few (1987), The electric field alignment of ice particles in thunderstorms, *J. Geophys. Res.*, *92*, 14,833–14,844, doi:10.1029/JD092iD12p14833.

Weiss, S. A., W. D. Rust, D. R. MacGorman, E. C. Bruning, and P. R. Krehbiel (2008), Evolving complex electrical structures of the STEPS 25 June 2000 multicell storm, *Mon. Wea. Rev.*, *136*, 741–756, doi:10.1175/2007MWR2023.1.

Wiens, K. C., S. A. Rutledge, and S. A. Tessendorf (2005), The 29 June 2000 Supercell observed during STEPS. Part II: Lightning and charge structure, *J. Atmos. Sci. Atmos.*, *62*, 4151–4177, doi:10.1175/JAS3615.1.

Williams, E. R. (1989), The tripole structure of thunderstorms, *J. Geophys. Res.*, *94*, 13,151–13,167, doi:10.1029/JD094iD11p13151.

Zikmunda, J., and G. Vali (1972), Fall patterns and fall velocities of rimed ice particles, *J. Atmos. Sci.*, *29*, 1334–1347, doi:10.1175/1520-0469(1972)029<1334:FPAFVO>2.0.CO;2.